Comparison of SAR-Derived Wind Speed With Model Predictions and Ocean Buoy Measurements

Frank M. Monaldo, Donald R. Thompson, Robert C. Beal, William G. Pichel, and Pablo Clemente-Colón

***Abstract*—As part of the Alaska synthetic aperture radar (SAR) Demonstration Project in 1999 and 2000, wide-swath RADARSAT SAR imagery has been acquired on a regular basis in the Gulf of Alaska and the Bering Sea. During 1998 and 1999, similar data were acquired off the East Coast of the United States as part of the StormWatch Project. The radar cross section measurements from these images were combined with wind direction estimates from the Navy Operational Global Atmospheric Prediction System model to produce high-resolution maps of the surface wind speed. For this study, 2862 SAR image frames were collected and examined. Averaged wind estimates from this data base have been systematically compared with corresponding wind speed estimates from buoy measurements and model predictions, and very good agreement has been found. The standard deviation between the buoy wind speed and the SAR estimates is 1.76 m/s. Details of the SAR wind extraction procedure are discussed, along with implications of the comparisons on the C-band polarization ratio.**

***Index Terms*—Marine boundary layer, marine wind speed, National Data Buoy Center (NDBC) buoys, NOGAPS model, synthetic aperture radar (SAR).**

I. Introduction

MARINERS who sail in coastal waters have long known that near surface wind speeds are highly variable. Unfortunately, there has been a lack of precise meteorological measurements to aid in the monitoring and prediction of high-resolution winds in coastal areas. Sporadic measurements by buoys are too spatially separated to capture this variability. The 25-km or poorer resolution offered by satellite scatterometers or passive microwave measurements, while excellent in the open ocean, is too coarse for coastal areas where such measurements are often contaminated by land returns. Spaceborne optical imagery, though often limited by clouds, has provided hints of the complicated nature of high resolution wind speed variability in coastal areas [1].

It is only recently that remote sensing has offered the routine, all weather capability of systematically measuring winds at subkilometer scale resolution. Spaceborne wide-swath synthetic aperture radar (SAR) offers this potential. The high-resolution of SAR imagery with the coverage afforded by a 500-km wide swath available from the Canadian SAR RADARSAT-1 [2] is ideally suited for coastal wind speed measurements.

The goals of the Alaska SAR Demonstration Project [3] and the StormWatch Project [4], both of which are sponsored by the U.S. National Oceanic and Atmospheric Administration (NOAA), Washington, DC, are to develop and demonstrate the ability to use wide-swath SAR imagery to produce high-resolution wind speed estimates in a timely fashion. During the winter of 1999–2000, RADARSAT SAR imagery was acquired at the Alaska SAR Facility (ASF), Fairbanks, processed into imagery, forwarded to NOAA in Camp Springs, MD, and used to produce wind speed estimates in near real time [5].

Thus far we have been able to produce such estimates in 5 to 6 h from acquisition to wind speed estimates posted on the world wide web. Of this time, approximately 2 h is required to produce a SAR image and about a half an hour is required to process a single frame into wind speed. Part of the remaining time is occupied in the data transmission from Alaska to NOAA for wind speed processing and cataloging the data. In addition, a single satellite overpass is broken up into image frames. The frames are processed in sequence. Hence, subsequent frames must remain in the processing queue until previous frames are processed.

The total time from satellite to data availability needs to be reduced to 2 to 3 h to be more useful in an operational context. One possibility is to eliminate data transmission time delays, by processing the imagery into wind speed at the SAR receiving station.

Fig. 1 is a sample wind speed map produced from RADARSAT-1 SAR imagery using a procedure to be discussed below. For this image the wind speed pixels are 1 km on a side. The retrieved SAR wind speeds are represented by color. The arrows represent the wind speeds and directions from the Navy Operational Global Atmospheric Prediction System (NOGAPS) model. The wind directions from the NOGAPS model, as described in the following, were used in the wind speed retrieval process. The land areas are shown as a shaded relief map.

This particular image was acquired on September 30, 2000, at 03:48 UTC in the vicinity of Cook Inlet, AK. It is representative of many of the features seen in the SAR wind imagery. There is intensified gap flow as the wind is channeled between the Kenai Peninsula and Kodiak Island by the local topography. In the lee of geographic features, wind shadowing is evident. Perhaps most interesting is the observation that wind speeds tend to be stable and coherent along the wind direction. However, in the cross wind direction there is often rapid variability in the wind speed. In this direction, wind speeds can change from near 0 to

Manuscript received January 19, 2001; revised July 23, 2001.

F. M. Monaldo, D. R. Thompson, and R. C. Beal are with the Ocean Remote Sensing Group, The Johns Hopkins University Applied Physics Laboratory, Laurel, MD 20723-6099 USA (e-mail: f.monaldo@jhuapl.edu; donald.thompson@jhuapl.edu; r.beal@jhuapl.edu).

W. G. Pichel and P. Clemente-Colón are with the Office of Research and Applications, Oceanic Division, National Environmental Satellite, Data and Information Service, National Oceanic and Atmospheric Administration, Camp Springs, MD 20746-4304 USA (e-mail: William.G.Pichel@noaa.gov; Pablo.Clemente-Colon@noaa.gov).

Publisher Item Identifier S 0196-2892(01)09905-3.

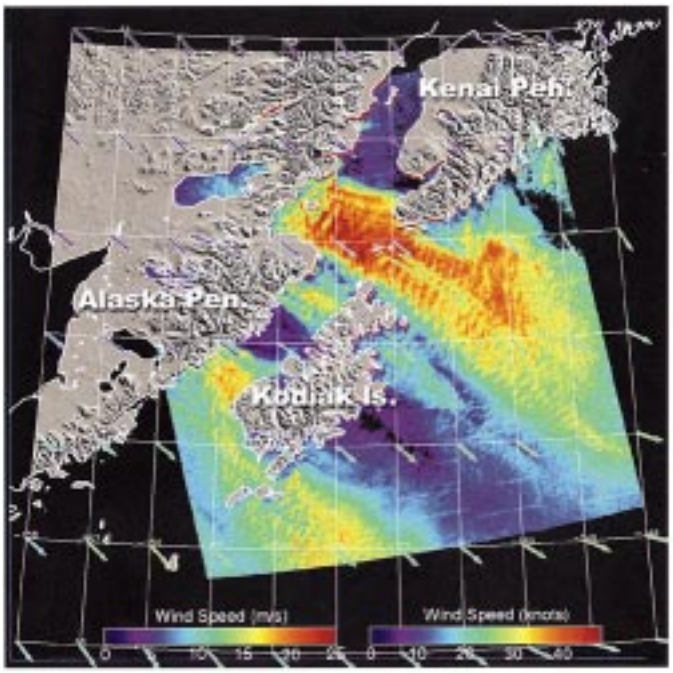

Fig. 1. Sample wind speed map computed with RADARSAT SAR imagery. The map is color-coded to reflect the SAR-retrieved wind speed. The orientation of the arrows represent the model wind direction. The color of the arrows represents the model wind speed. Land is shown as a shaded relief map. The wind speed pixels are 1 km on a side. The NOGAPS model directions are used in the wind speed retrieval process.

20 m/s over a few kilometers. Images like these underscore the value of high-resolution wind speed images in coastal areas.

In addition to the images acquired as part of the Alaska SAR Demonstration, during the StormWatch project RADARSAT wide-swath SAR imagery was also acquired off the East Coast of the United States where numerous National Data Buoy Center (NDBC) buoys are located. Taken together, these data sets provide an important opportunity to validate the accuracy of the retrieval of high-resolution wind speed from SAR imagery.

II. Road From Radar Cross Section to Wind Speed

The challenge in estimating wind speed from SAR radar cross section measurements is two fold. First, we must be able to specify the relationship between ocean surface wind velocity and normalized radar cross section (NRCS), the geophysical model function (GMF). Second, the SAR directly measures only backscattered power from which NRCS is determined. A particular NRCS estimate may correspond to a range of wind speeds depending on the angle between the radar look direction and the wind direction. Hence, in order to perform the wind speed inversion, we must first specify the wind direction.

The development and launch of the C-band, VV-polarization (VV-pol) wind scatterometer aboard the ERS-1 satellite necessitated the development of a well-validated scatterometer GMF for this system. At present, the most commonly used GMF is the CMOD4 GMF [6] that specifies the VV-pol NRCS, $\sigma^0_{\rm V}$ in terms of the wind vector and radar geometry with an equation of the form

$$\sigma^0_{\rm V} = a(\theta) U^{\gamma(\theta)} \left[1 + b(\theta)\cos\phi + c(\theta)\cos 2\phi\right] \qquad (1)$$

where

- θ local incident angle;
- U wind speed (usually assumed to be measured at 10 m above the surface with neutral atmospheric stability);
- $\gamma(\theta)$ power law dependence on wind speed;
- ϕ angle between the radar look direction and the wind direction.

When the radar is looking into the wind ($\phi = 0$), the NRCS is a maximum. Since $\gamma(\theta) > 1$, (1) indicates that the NRCS increases with wind speed. The NRCS also increases with decreasing incident angle. The CMOD4 GMF has been validated during numerous experimental campaigns for incident angles in the range from about 20° to 60° [6].

There is no similarly validated scatterometer GMF that relates the HH polarization (HH-pol) NRCS of the RADARSAT-1 SAR to wind. To deal with this deficiency, we employ a polarization ratio following the development of Thompson *et al.* [7] and Thompson and Beal [8]. This development relates the HH-pol NRCS, $\sigma^0_{\rm H}$, to $\sigma^0_{\rm V}$ through the equation

$$\sigma^0_{\rm H} = \left(\frac{1 + \alpha \tan^2\theta}{1 + 2\tan^2\theta}\right)^2 \sigma^0_{\rm V} \,. \qquad (2)$$

The polarization ratio is a function of incident angle and the parameter α. For $\alpha = 0$, the polarization ratio $\sigma^0_{\rm H}/\sigma^{\rm V}_0$ given by (2) is that predicted by Bragg scattering theory, while for $\alpha = 1$, (2) produces the value for $\sigma^0_{\rm H}$ predicted by Kirchhoff (physical optics) scattering [7]–[9]. Thompson *et al.* and Thompson and Beal [8] proposed $\alpha = 0.6$ based on airborne measurements of the HH-pol NRCS collected by Unal *et al.* [10] at several incident angles and a range of wind speeds. Vachon and Dobson [11] compared RADARSAT SAR-derived wind speeds with buoy measurements and suggested $\alpha \simeq 1$. Horstmann *et al.* [12], [13] compared RADARSAT SAR wind speeds with ERS-2 scatterometer wind speed measurements and a high-resolution local wind speed model. They determined that $\alpha \simeq 1$ as well.

We suspect that the polarization ratio may also be dependent upon relative look direction ϕ. However, such a relationship has not been developed for this frequency. While it may be possible to infer such a relationship from the data we have acquired, this work is beyond the scope of this paper. In addition, uncertainties in the NRCS may hinder or limit the general applicability of any such polarization ratio function developed with these data.

For the wind speed retrievals derived from RADARSAT SAR imagery to be discussed in the present paper, we choose $\alpha = 0.6$ in (2). Besides the HH-pol airborne measurements of [10] that point to such a value for α, we will show in the following discussion that this choice is consistent with comparisons between SAR-derived wind speeds and both model and buoy estimates. In addition, we will show that choice of α that produces the best agreement is very sensitive to the NRCS calibration as well as to the method used to compute the local incident angle in the wide-swath SAR image. As a consequence, when investigators attempt to choose an empirical α value, they may simply be using the α parameter in (2) to tune the wind speed retrievals for differences in calibration or even angles of incidence.

A. Wind Direction

For any particular pixel in a SAR image, we know the radar cross section and the local incident angle. In order to invert (1) and (2) and estimate wind speed, we begin with an *a priori* estimate of the angle between the wind direction and the radar look direction. There are two general approaches to obtaining this estimate: 1) use structures in the SAR image to infer wind direction or 2) obtain wind direction from a wind field model.

As long ago as 1986, Gerling [14] demonstrated that linear features in Seasat SAR ocean imagery on the scale of a kilometer or larger may be the result of wind-induced features that are correlated with local wind direction. More recently, Fetterer *et al.* [15] and Muller *et al.* [16] have used wind directions derived from such features in ERS-1 SAR imagery to estimate wind direction and combined these directions with the VV-pol NRCS measurements from ERS-1 to estimate wind speed. Presently, Wackerman [17] is also using wind directions derived from RADARSAT SAR images from the Alaska SAR Demonstration to estimate wind speed.

Although useful and convenient, the use of linear features in the SAR image to estimate wind direction can sometimes lead to erroneous results. Wind-induced signatures such as wind rows are most conspicuous under unstable atmospheric conditions, but in some cases, especially in neutral or stable conditions, they are not present at all. In addition, there can be other features in SAR images, such as oceanic or atmospheric internal waves, that produce linear features on the same spatial scale as wind rows. These other features are not generally aligned with the local wind vector and can contaminate this method of estimating the wind direction directly from the SAR image itself.

An alternate approach is to use wind direction estimates from meteorological forecast models in the generation of SAR wind maps. The virtue of using model wind directions in the retrievals is that they always produce physically reasonable estimates of the wind direction field. However, the model wind directions are themselves also not always correct and are not generally produced at the high (1 to 10 km) resolution most useful for this application.

In this paper, we use model wind directions as produced by the NOGAPS model to determine wind direction. For future refinement of our present procedure, we believe the best solution to the wind direction question will probably be a thoughtful and careful combination of the wind directions derived from the images themselves constrained by direction fields from high-resolution meteorological models.

B. Wind Speed Retrieval Procedure

As part of the Alaska SAR Demonstration Project, we have been processing SAR imagery from ASF to produce high-resolution estimates of wind speed. This procedure involves merging data from two sources: the SAR imagery from ASF and the model fields from the NOGAPS model. SAR imagery from the Alaska region that falls within the real-time reception mask of ASF is correlated at ASF to produce calibrated wide-swath SAR imagery. These data are then electronically forwarded to NOAAs Satellite Active Archive (SAA). From there the data are automatically forwarded to NOAAs National Environmental Satellite Data and Information Service (NOAA/NESDIS) and the Johns Hopkins University Applied Physics Laboratory (JHU/APL). In addition, the US Navy's Master Environmental Library (MEL) forward to NOAA/NESDIS and JHU/APL the NOGAPS model winds. These model wind fields include both forecasts and nowcasts.

At both NOAA/NESDIS and JHU/APL, we run parallel software to produce SAR wind speed estimates and post these results on the World Wide Web. (The web sites at NESDIS and JHU/APL are: orbit35i.nesdis.noaa.gov/orad/sar/ and fermi.jhuapl.edu/sar/stormwatch/, respectively.) Once the SAR data arrive at either NOAA/NESDIS or JHU/APL, processing automatically begins. We have generally been averaging the SAR data from their original 100 m pixel spacing to 600 m, though to decrease processing time 1000 m pixels have been used as well. Contamination of the wind-speed statistics in the SAR wind maps due to oceanic processes of the same scale as the wind fluctuations as well as SAR speckle noise limit the highest useful resolution to about 300 m [18]. At each image pixel, we linearly interpolate a model wind direction from the $1^\circ \times 1^\circ$ longitude-latitude grid of the NOGAPS model to the geographic position of the pixel. Using this model direction and the SAR radar cross section at the pixel of interest, we then invert (1) and (2) to compute the associated wind speed [5], [8]. It typically takes 5 to 6 h from reception of data at the satellite to the posting of the wind speed maps on the web. However, an improvement to less than two hours is technically feasible, particularly if the wind processing and web posting are relocated to the SAR receiving station.

III. Comparison of Model Wind Speeds and SAR Wind Retrieval

The aim of the work described herein is to validate the usefulness of high-resolution wind speeds produced from wide-swath SAR imagery. The wind speeds from global models, while coarse in resolution, provide useful indicators of potential systematic problems in the SAR-derived wind speeds. Although it is likely that the point-by-point differences between the model and SAR-derived wind speeds are large, certain systematic differences can be used to diagnose the SAR-retrieval procedure. The additional virtue of SAR versus model comparisons is that there are many of them. For the comparisons discussed below, we gathered data from 2862 SAR image frames for data spanning the years 1997 to 2000. From these, we accumulated 7290 model and SAR wind-speed comparisons at the model grid points. At each position, we averaged the SAR wind speed over a 50 km $\times$ 50 km square area to make the result more consistent with the spatial averaging inherent in the model estimate.

To insure that we examine only marine wind speeds and not accidently consider NRCS measurements over land, we have carved out an area in the Gulf of Alaska region. The Alaska SAR Demonstration Project provides extensive SAR coverage of this area. Fig. 2 presents NRCS as a function of angle of incidence for the 7290 comparisons. Each diamond value represents the mean radar cross section averaged over a 1° incident

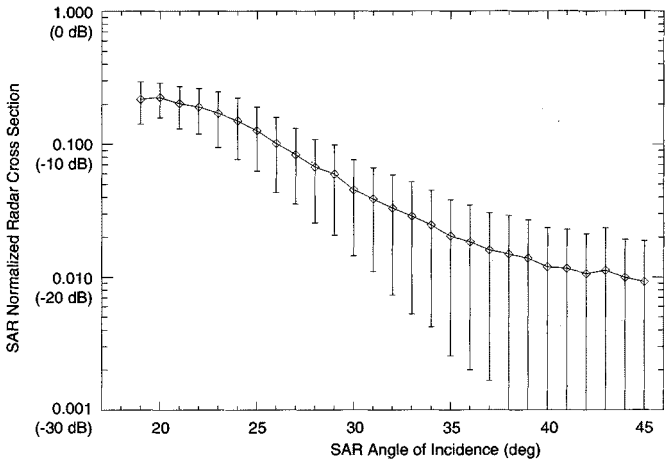

Fig. 2. Normalized radar cross section as a function of incident angle for 7290 points obtained from RADARSAT SAR wide swath imagery as processed by ASF. The diamonds represent the mean cross section in 1° increments, and the error bars show the ± one standard deviation limits.

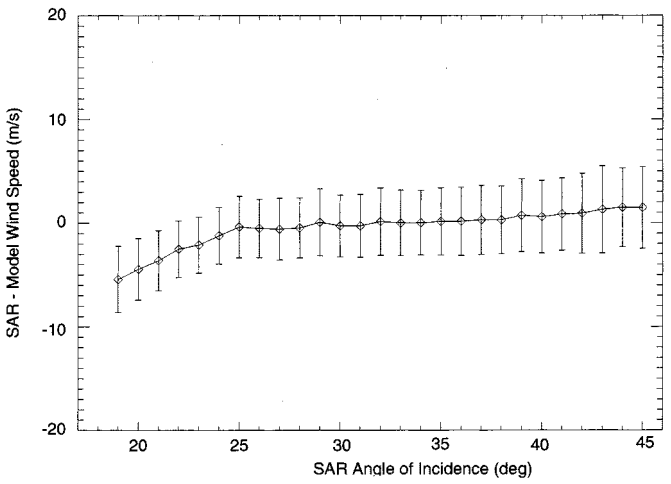

Fig. 3. Difference between SAR-derived and model wind speed function of incident angle for 7290 points obtained from RADARSAT wide swath imagery as processed by ASF. The diamonds represent the mean cross section in 1° increments, and the error bars show the ± one standard deviation limits.

angle bin. The error bars represent the plus-or-minus one standard deviation limits within each of these bins and reflect the corresponding variability in wind speed and direction.

A. Near Range Problems With Radar Cross Section

For a fixed wind speed, we expect NRCS to increase with decreasing angles of incidence. This trend is most pronounced near 20° incidence and persists in a mean sense even when the winds are variable. The retrieved NRCS from our data base of ASF-processed wide-swath SAR imagery shown in Fig. 2 does not exhibit this expected behavior for incident angles less than 25° or so. At these angles, one can see from the figure that the retrieved NRCS values level off rather than rapidly increase. This problem manifests itself in the form of lower than expected wind speeds from our wind inversion procedure at near-range incident angles. This near range problem has been noticed in RADARSAT SAR imagery by others [19], [20] and has been associated with analogue-to-digital converter saturation.

Fig. 3 is a plot of the difference between the SAR-derived and model wind speeds as a function of incident angle. All winds are scaled to 10 m height and neutral atmospheric stability. The diamonds represent data averaged in 1°-bins. Note the reduced SAR wind speeds in the near range. It is possible to make an *ad hoc* polynomial correction to the SAR wind retrieval as a function of incident angle to force the SAR wind speeds to be in greater conformity with the model speeds. We have, however, not applied such a correction to the results presented in this paper.

It is interesting to note that the standard deviation of the difference between the SAR-derived and model wind speeds slightly increases with increasing incident angle. The derivative of wind speed with respect to NRCS increases with incident angle. We suspect that similar levels of NRCS noise at far range incident angles may be associated with more noise in the SAR-derived wind speed. In addition, the calibration of NRCS may be more difficult and hence less accurate in the far range.

B. Tuning the Polarization Ratio

There is some controversy as to the value of α in (2) to be used in computing the wind-speed dependence of σ^0_{H}. We used comparisons of model and SAR wind speed estimates made at a variety of different α's to determine the α-value that minimizes the difference in these comparisons. Using the data base of model and SAR wind speeds described above, we have excluded for the purposes of this comparison SAR wind speeds acquired at incident angles less than 25°. This latter constraint excludes data possibly contaminated from the near-range problems in NRCS discussed earlier. Altogether, the resulting data base includes 4273 model-SAR wind speed comparisons.

Fig. 4 presents six plots of the SAR and model wind speed probability density functions (PDF's) computed using various α values. The thick line, representing the model wind speed PDF, is constant in all the plots. The thinner line is the PDF of the associated SAR wind speeds. For $\alpha = 0$, the mean SAR wind speed is 11.18 m/s compared to the model mean of 8.03 m/s. At the opposite extreme for $\alpha = 1.0$, the mean SAR wind speed of 6.57 m/s is lower than the model mean. For $\alpha = 0.6$, the mean wind speeds from the SAR and the model match most closely. The evidence from these comparisons suggests that it is appropriate to continue to use α in (2) in our wind-speed retrievals.

Fig. 5 shows a set of contour plots of the magnitude of the difference between SAR-derived and model-estimated wind speed (plotting each of the 4273 individual points in standard scatterplot format yields plots that are difficult to read.) There are ten linearly-spaced contours in each plot in Fig. 5. Perfect agreement occurs when the contours collapse along the 45° line. The scatter is relatively large with standard deviations of about 4 m/s.

Typically, the time difference between the SAR wind speed measurements and the model prediction time can be six hours. Monaldo [21] found that time separations of this order can lead to standard deviations of up to 3 m/s between wind speed measurements. Also, given the fact that the SAR is picking up more of the local variability smoothed over by the model estimates and error in the GMF, the scatter is not entirely unexpected.

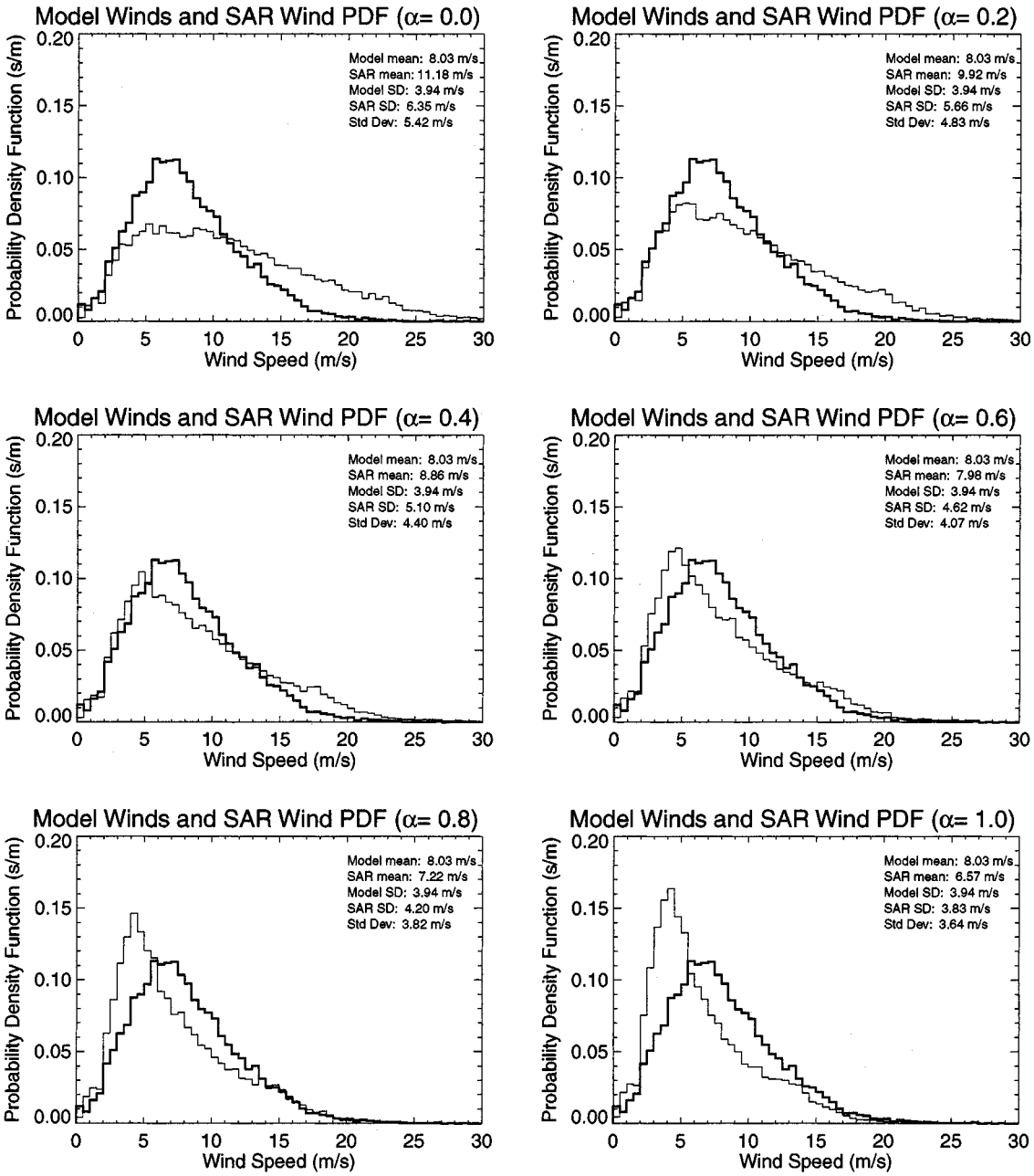

Fig. 4. Comparison of SAR and NOGAPS model wind speed PDFs for different values of α. The thick line represents the model wind speed PDF. The thin lines represent the SAR wind PDF's. The SAR and model standard deviations are with respect to their respective wind speed distributions. The last listed standard deviation in each plot is the standard deviation of the difference between the SAR and model wind speed at every comparison point.

Nonetheless, the large number of comparisons included in the plots in Fig. 5 again confirms that a choice for the α parameter near 0.6 yields the most satisfactory agreement.

IV. Buoy Comparisons

A. NDBC Buoy Data Set

The NDBC deploys and maintains a set of buoys in coastal US waters [22]. In our comparisons of the SAR-derived wind speeds with measurements from these NDBC buoys, we have used only data from buoys that are sufficiently far from land that the SAR wind speed retrievals (including a 3 km $\times$ 3 km area average centered on the buoy location) will not include image pixels intersecting land. This averaging area roughly corresponds to the distance covered by wind at 7 m/s over the 8-min averaging time of a buoy.

Fig. 6 is a plot of the buoy locations used in these comparisons. The crosses in this figure indicate the geographic location of the buoy. The adjacent numbers represent the number of buoy-SAR comparisons available from the associated buoy. Since the East Coast of the United States has such a high density of buoys, most of the comparison pairs are located there. The buoy comparisons include data from our RADARSAT SAR wide-swath database in the time interval from November 1997

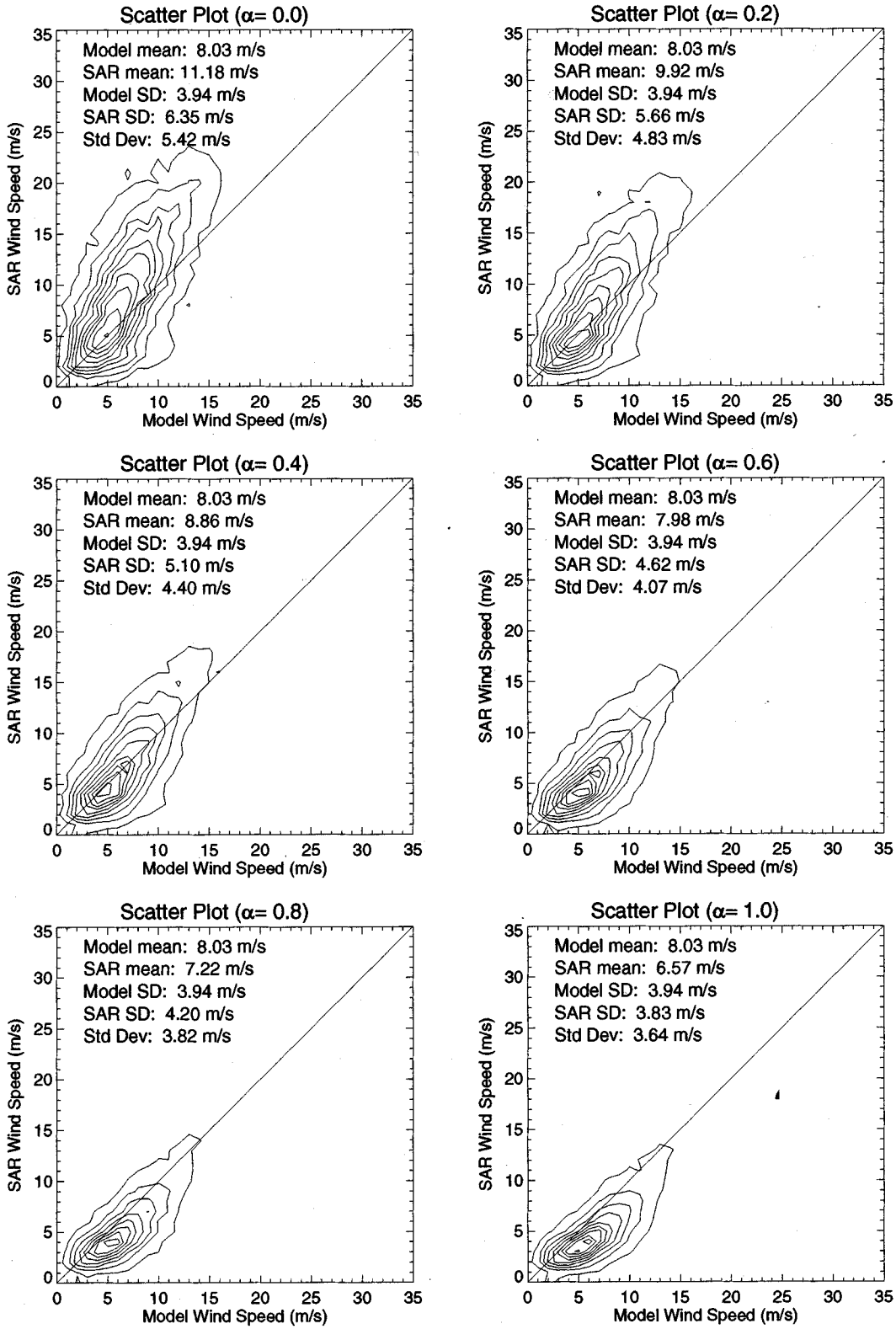

Fig. 5. Scatter plots of SAR-estimated wind NOGAPS model wind speed for different values of α. The data are represented as contour plots rather than as individual points. The 45° line represents perfect agreement. The SAR and model standard deviations are with respect to their respective wind speed distributions. The last listed standard deviation in each plot is the standard deviation of the difference between the SAR and model wind speed at every comparison point.

to November 1999 and include 317 SAR-buoy potential comparison pairs in the 18° to 45° incident angle range.

Buoy wind speed measurements are generally reported on the hour and represent 8-min averages. Hence, SAR and buoy comparisons are never separated in time by more than 30 min. An inherent limitation in any comparison presented here is the fact that a buoy averages wind speed over time, while the SAR averages over an area. These two averages may not always be

Fig. 6. Map of buoy locations associated with at least one SAR-buoy comparison pair. The crosses indicate the locations. The numbers represent the number of buoy-SAR wind speed comparisons available for the buoy location.

interchangeable. Also, in generating the comparison database, we have taken care to adjust the wind speeds measured directly by the buoy to equivalent neutral stability wind speeds at 10 m height. The adjustment to 10 m height was generally the most important component of this procedure. The TOGA-COARE bulk flux algorithm [23] has been used for the stability correction and results in relatively small changes except for wind speeds less than about 3 m/s.

B. Differences Between SAR and Buoy Wind Speeds

Fig. 7 is a plot of the SAR-retrieved wind speed versus buoy-estimated wind speed using this averaging procedure. The standard deviation is 1.83 m/s with a bias of 1.06 m/s. For this plot, we included incident angles from 18° to 45°.

Fig. 8 is the same as Fig. 7 except that incident angles less than 25° are excluded to eliminate comparisons for which the radar cross section may be underestimated as discussed previously. This constraint reduces the number of SAR-buoy comparison pairs to 260. Note that the magnitude of the mean difference is reduced from 1.06 m/s to 0.85 m/s and the standard deviation is falls to 1.76 m/s.

Of course, there are a number of reasons for the residual differences between the buoy and SAR wind speed measurements. Besides potential inaccuracies in NRCS, there remains the possibility that the CMOD4 GMF and polarization ratio functions used here require further refinement. One significant reason for residual differences is any error in the wind direction used in the SAR wind speed retrieval. This is discussed below.

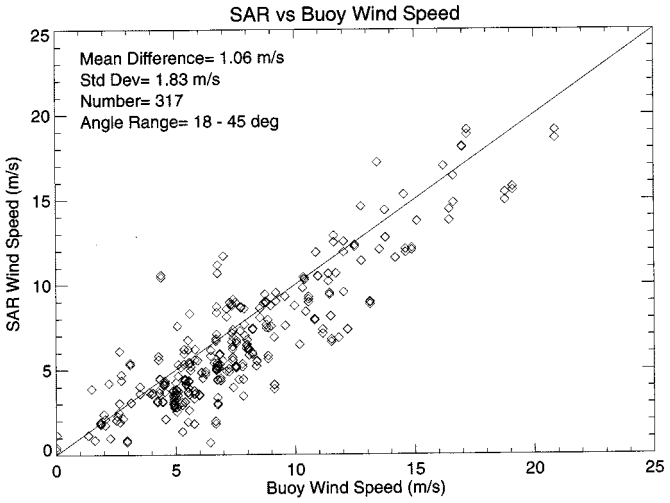

Fig. 7. SAR versus buoy-estimated wind speed for incident angles 18° to 45°. For this comparison, an α-parameter value of 0.6 has been used.

C. Wind Direction Comparisons

The SAR wind-speed retrieval is dependent upon the accuracy of wind directions from the NOGAPS prediction model. Differences between the actual direction and the inferred wind direction from the model may contribute to differences between

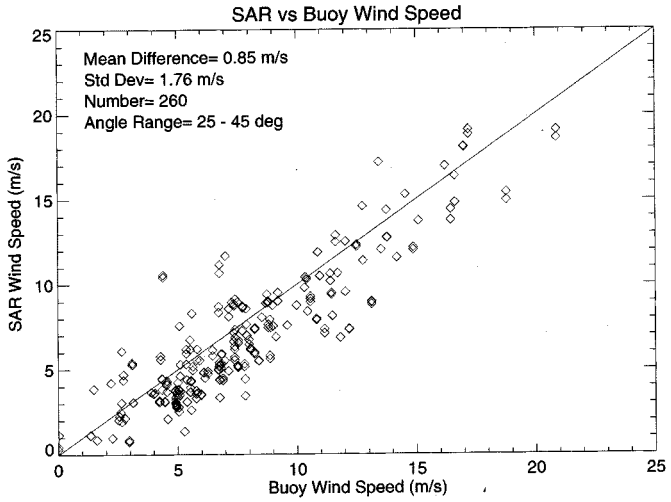

Fig. 8. SAR versus buoy-estimated wind speed for all incident angles between 25° and 45°. For this comparison, an α-parameter value of 0.6 has been used.

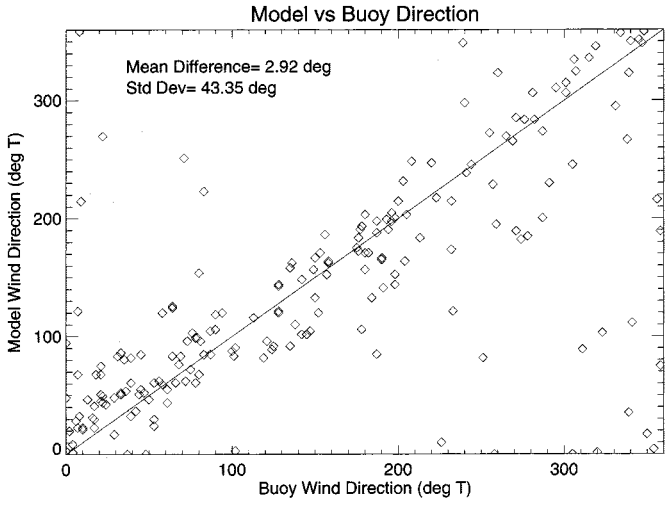

Fig. 9. Model-estimated wind direction versus buoy-estimated wind direction.

SAR-estimated wind speed and buoy wind speed. Fig. 9 is a scatter plot that compares the NOGAPS model wind direction with the buoy-estimated wind direction. The mean difference in wind direction is small; less than 3°. However, the standard deviation of the difference between buoy and model wind direction is a significant 44° and certainly accounts for some of the scatter in SAR versus buoy comparisons. The buoy data set used here provided a wide distribution of wind directions for validation purposes.

In order to assess the effect of potential errors in wind speed caused by errors in the *a priori* wind direction from NOGAPS, we have recomputed the SAR wind speeds for the buoy comparisons using the wind direction reported by the buoy itself. The results of this comparison are shown in Fig. 10. The mean difference 0.61 m/s is a bit smaller, but the standard deviation 2.32 m/s is almost 50% higher than when the model wind directions were used. (See Fig. 8.) We suspect this increase in standard deviation may be due to the fact that buoy wind direction estimates contain local fluctuations not present in the model fields.

How important is it to have a reasonable estimate of wind direction in the retrieval process? We have attempted to assess

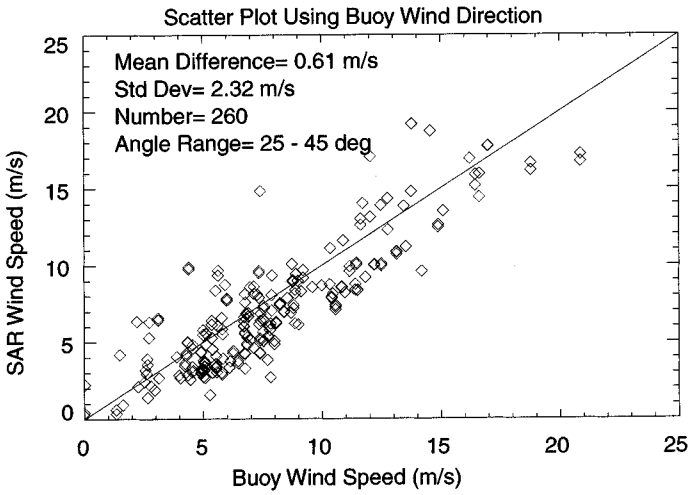

Fig. 10. SAR wind speed retrievals as a function of the buoy estimate using buoy-reported wind directions in the SAR wind speed retrieval. Incident angles between 25° and 45° and an α-parameter value of 0.6 were used in this comparison.

this question by using fixed wind directions in conjunction with the SAR radar cross section measurement instead of the model direction to estimate the SAR wind speeds. Fig. 11 shows the results for various (fixed) wind directions and $\alpha = 0.6$ for each case. The standard deviation between the SAR and buoy wind speeds under these conditions changes depending on the particular wind direction assumed. Perhaps the best case (based on the smallest mean difference) is when the wind direction is set to 300°. Note the standard deviation for this case of 2.34 m/s is significantly higher than the value of 1.76 m/s obtained when we used the model wind directions. Despite the increase in standard deviation, credible (mean) wind speed retrievals may sometimes be possible using a reasonable *constant* estimate of the wind direction. However, we believe that neglecting to use the model wind directions will generally produce a significant degradation in the retrieved wind field.

D. Implication of the SAR Buoy Comparisons on α

Comparisons between SAR and buoy measurements can also reveal useful information about the optimum choice for α in the wind speed retrieval. Fig. 12 shows a series of scatter plots of SAR versus buoy wind-speed comparisons using different values of α in the SAR inversion. For these comparisons, the NOGAPS model wind directions were used and only those incident angles in the range $25° \leq \theta \leq 45°$ were included. Note that the minimum (magnitude) mean difference of 0.01 m/s occurs for $\alpha = 0.4$, though the standard deviation for this case is 1.93 m/s. At $\alpha = 0.6$, the mean difference is larger, but the standard deviation drops to 1.77 m/s. At still higher α's, the mean difference grows larger, though the standard deviation does not appreciably change. The results shown in Fig. 12 suggest again that setting α to 0.6 produces the best compromise in mean difference and standard deviation in SAR versus buoy wind speed comparisons. For values of α significantly higher or lower than 0.6, the mean error becomes unacceptably large.

We should note that the choice of α can be affected by relatively small biases in the SAR NRCS. To obtain the NRCS

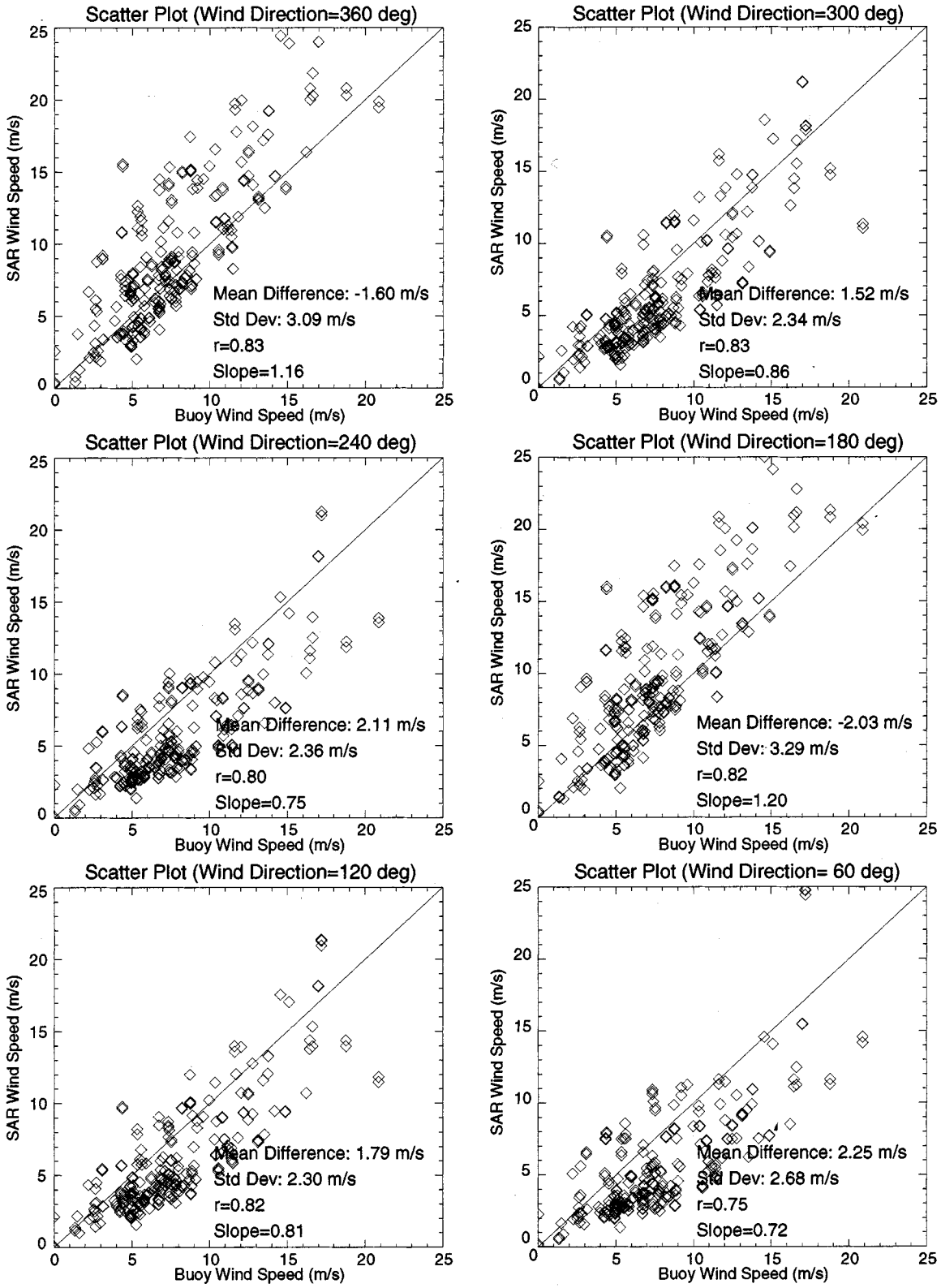

Fig. 11. SAR wind speed retrievals as a function of the buoy estimate using for various fixed wind directions for the SAR speed retrievals. Incident angles between 25° and 45° and an α-parameter value of 0.6 were used for each case.

at each pixel in the image, we use the calibration schemes employed by the Alaska SAR Facility. It is important to realize however, that there are potentially small biases between RADARSAT SAR NRCS produced by different SAR image processing facilities. Moreover, biases may also be introduced by the specific technique used to compute the local incident angle at the position of interest in the SAR image. This computation is relatively straightforward given accurate specification

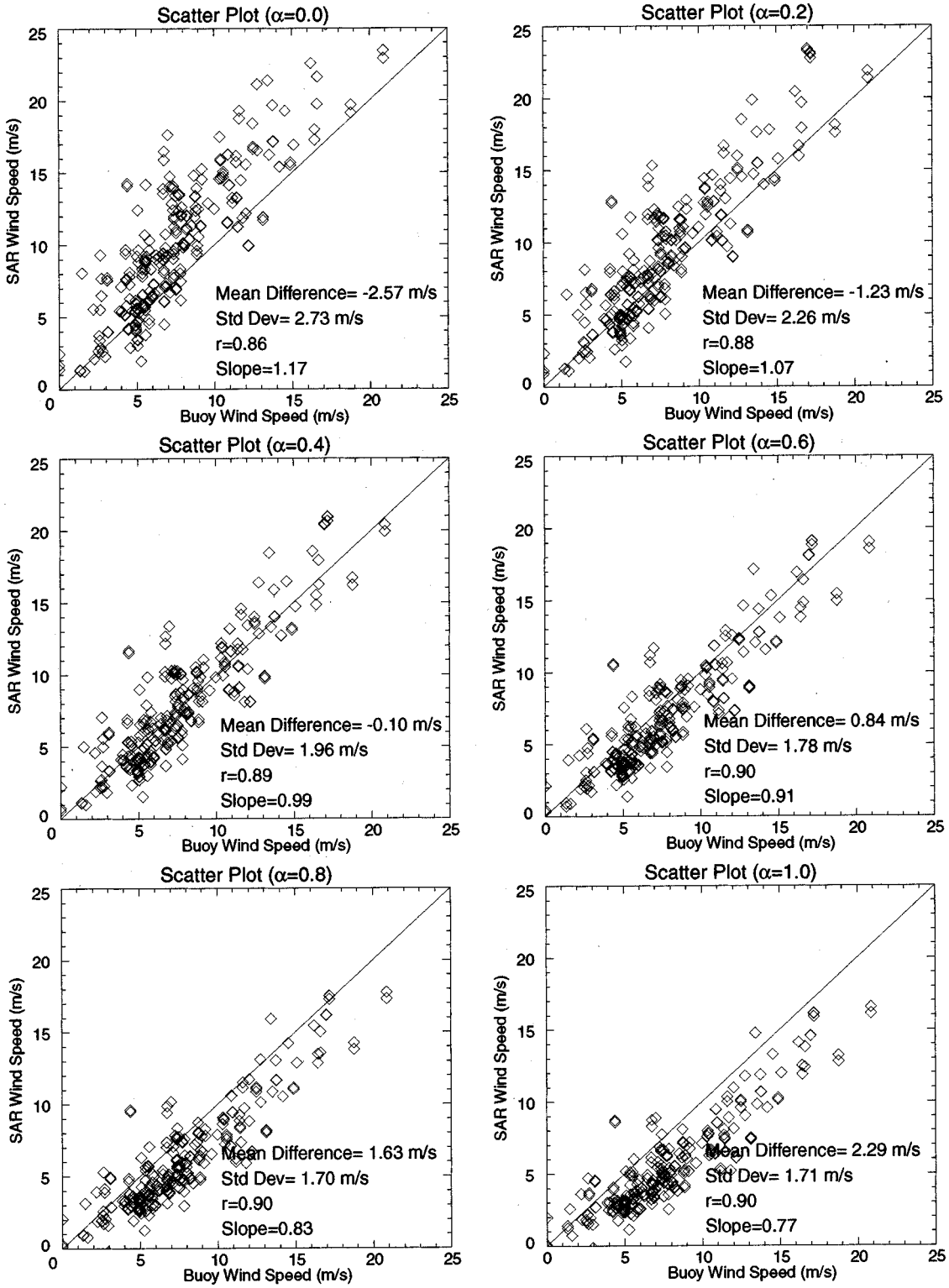

Fig. 12. SAR wind speed retrievals as a function of the buoy estimates using different value of α in the SAR wind speed retrieval. NOGAPS model wind directions were used in each of the plots.

of the satellite location, but the effect of the Earth's curvature must be included. This is particularly important in the case of wide-swath SAR imagery. In addition, the SAR imagery processed at ASF at northern latitudes are usually resampled into polar stereographic coordinates. Associating particular image pixels with incident angle becomes correspondingly more difficult.

As various investigators try to determine α by comparisons with independent wind speed estimates, all should be aware this sensitivity of the α-value to small differences in the NRCS algorithms and also in the scheme for computing incident angle. The analyses of Vachon and Dobson [11] and Horstmann *et al.* [12] that suggested $\alpha \simeq 1$ for example, were performed with SAR radar cross section images generated at facilities other than

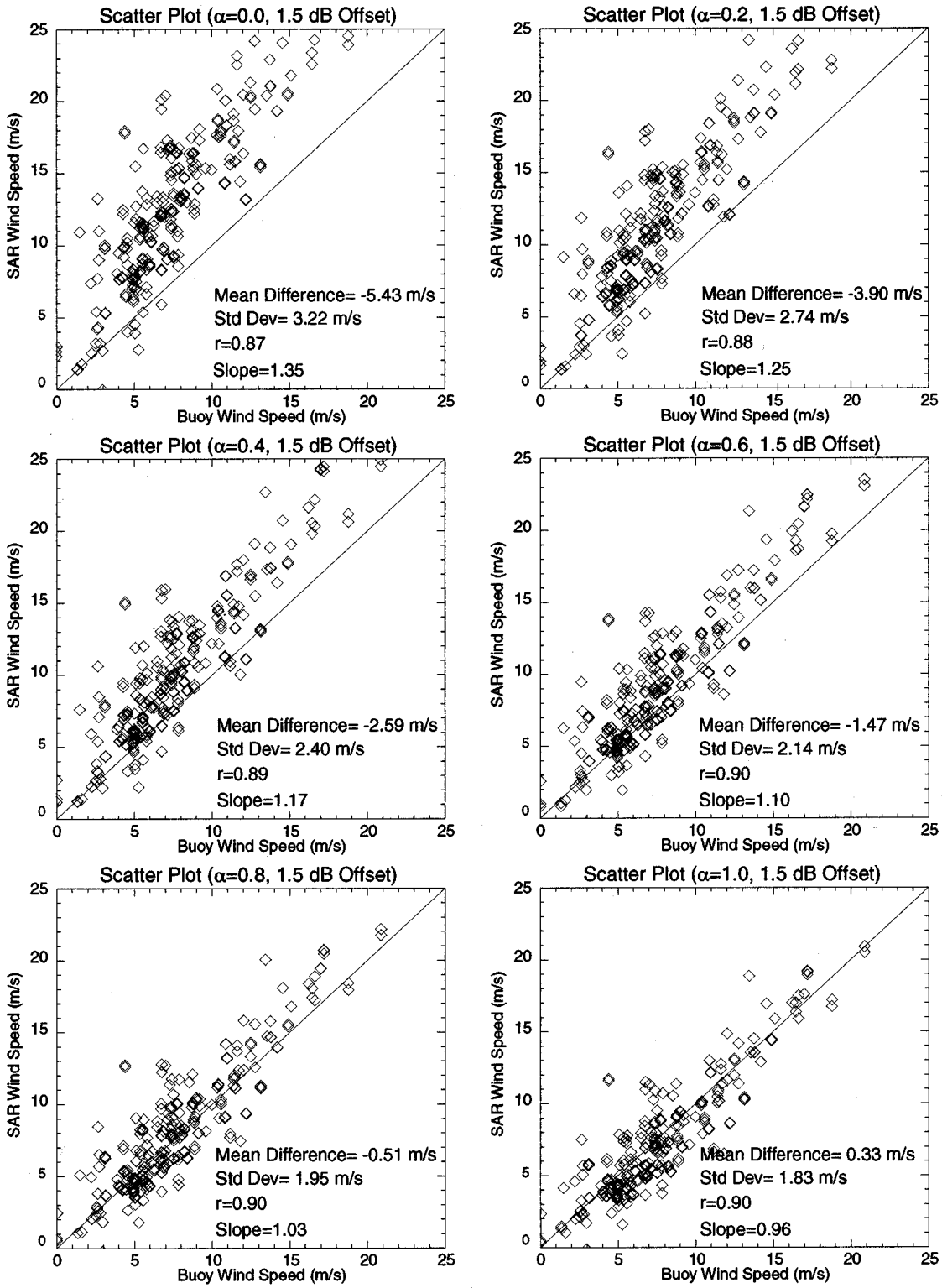

Fig. 13. SAR wind speed retrievals as a function of the buoy estimates using different value of α in the SAR wind speed retrieval. The radar cross sections were biased by 1.5 dB. SAR data for incident angles between 25° and 45° were included. The wind directions were obtained from the NOGAPS model.

ASF. Small differences in the NRCS between these other facilities and ASF could manifest themselves in the form of different optimum α values. In Fig. 13, we show plots of SAR versus buoy wind speed for different α-values after biasing the NRCS in each case by 1.5 dB. As in earlier examples, only incident angles in the range $25^\circ \leq \theta \leq 45^\circ$ were included and the NOGAPS model wind directions were used. These plots show that if the NRCS at each pixel is biased high by 1.5 dB with respect to the corresponding ASF value, one could conclude from Fig. 13 that 1.0 is the optimum α value.

Similarly, modest errors in the computation of incident angle can account for different determinations of α. Fig. 14 shows

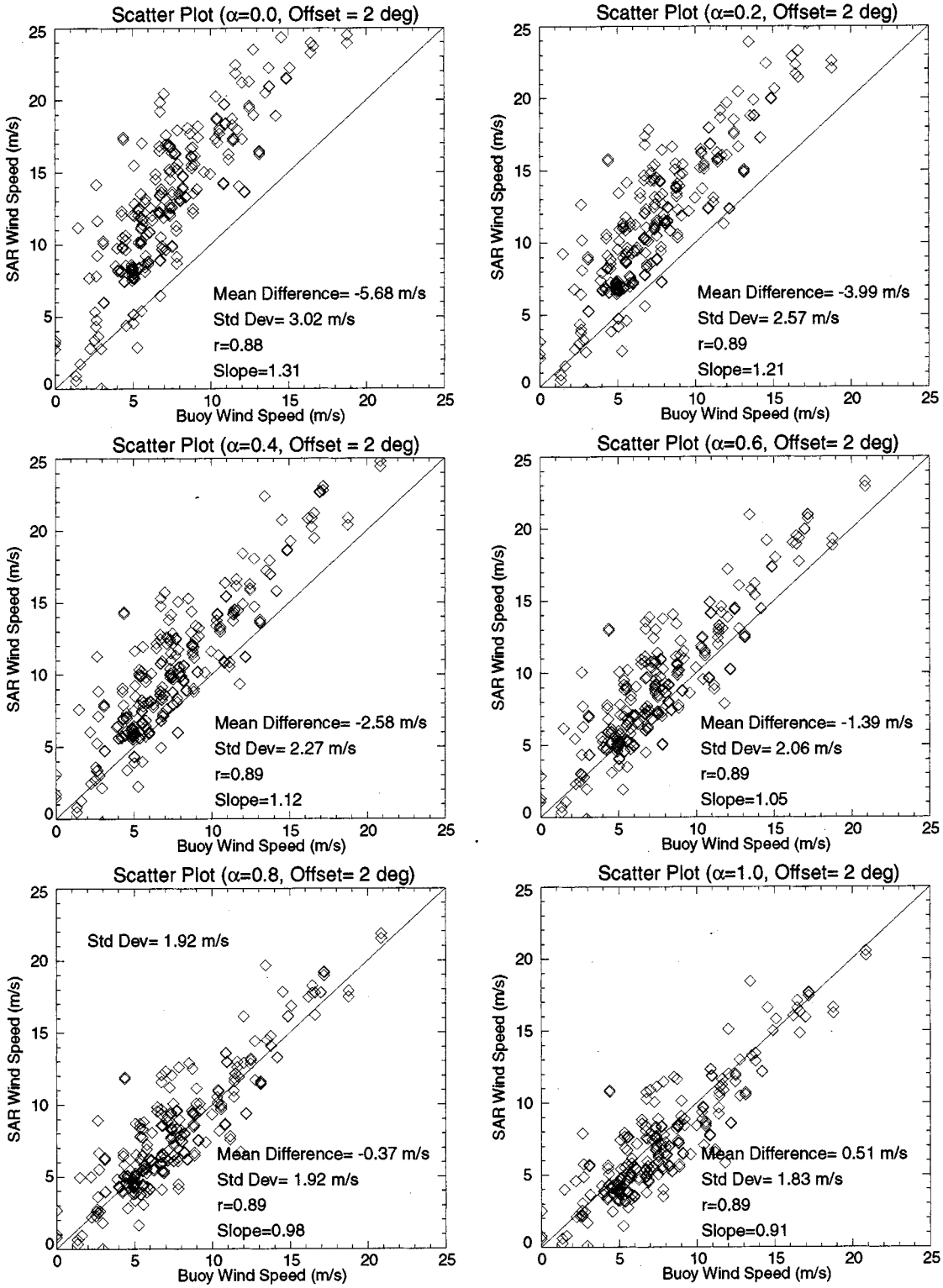

Fig. 14. SAR wind speed retrievals as a function of the buoy estimates using different values of α in the SAR wind speed retrieval. The incidence angles were biased by 2°. SAR data for incident angles between 25° and 45° were included. The wind directions were obtained from the NOGAPS model.

plots of SAR versus buoy wind speed for various α values computed after applying a bias of 2° to the incident angle. For this case, $\alpha = 1$ again produces agreement between SAR-derived and buoy wind speeds. Although we do not expect errors this large, it is clear that care must be taken the computation of incident angle.

Careful data handling is essential to avoid errors originating from an incorrect NRCS or incident angle when attempting to determine the proper value of α. Simultaneous VV- and HH-pol imagery from ENVISAT [24] to be launched in June 2001 should help significantly in the clarification of this issue. Given Unal's experimental results [10] and the fact that an

$\alpha = 0.6$ seems to provide close to optimum results when SAR-derived wind speeds are compared to buoy wind speeds, we see no reason to deviate from this choice for the α value.

V. Conclusions

For the first time, we have been able to make systematic comparisons of a large number of buoy and model wind speed estimates with coincident estimates of wind speed from a spaceborne SAR. Wind directions used in the retrieval process were obtained from the operational NOGAPS model. Comparisons of SAR-derived wind speeds with buoy measured wind speeds indicate that a properly calibrated SAR can be used over the ocean as a high spatial resolution anemometer.

Although we have found a systematic underestimate of radar cross section for incident angles less than 25°, the standard deviation in wind speed retrievals is as low as 1.76 m/s. Some of the differences between the buoy and SAR wind speeds are due to uncertainties in the wind direction. Moreover, variability in the sampling between an instrument like a SAR that averages over area and a buoy that averages over time can also contribute to the differences.

The comparisons discussed in this paper indicate a value for the α parameter in (2) around 0.6, in general agreement with the measurements of Unal *et al.* [10]. In spite of this agreement with the buoy- and model-derived wind speeds, some questions remain. As we have pointed out, Vachon and Dobson [11] and Horstmann *et al.* [12], [13], have found that a value for α close to unity gives better agreement in their SAR wind-speed inversion. As these authors mention and as we have demonstrated in the present paper, calibration uncertainties as well as slight inaccuracies in computation of the local angle of incidence could partially account for the apparent discrepancy between our findings and theirs. In any case, it is clear that present knowledge of the C-band polarization ratio is inadequate. Even at moderate incidence angles, measured values for this ratio are larger than those predicted by the rough-surface scattering models commonly in use. At 45° incidence for example, the measured HH/VV ratio for a 10 m/s wind directed toward the radar is about -3.5 dB at Ku-band and about -5.5 dB or so at C-band [10]. Bragg-based scattering models predict the HH/VV ratio at 45° to be about -9.5 dB, independent of radar frequency [7]. Ratios predicted by composite-type scattering models that include the effects of long-wave tilt and hydrodynamic modulation yield some improvement [25], but the predicted polarization ratios from these models generally remain too small.

The ENVISAT ASAR in its alternating polarization mode will have the capability to collect virtually simultaneous dual-polarization images covering a wide range of incidence angles [24]. We believe that this imagery when coupled with accurate environmental characterization will offer a unique opportunity to improve our understanding of the polarization-ratio discrepancy discussed above. By using descending overpasses along the eastern U.S. coast roughly between the Grand Banks and Cape Hatteras, NC, we can ensure that several NDBC data buoys are located within each SAR scene. When the imagery becomes available in the fall of 2001, we plan to compare trends in the ratio of ENVISAT HH- and VV-pol SAR scenes as a function of incident angle with predictions from rough-surface scattering models [9], [25] as well as with commonly used C-band scatterometer wind algorithms (mostly VV-pol to date [6]). Since both of these comparisons require measurements of the local wind vector (and air–sea temperature difference if available), the requirement that the NDBC buoys be located within the scenes is again very important.

Because of its high-resolution imaging capability, we believe that SAR scatterometry can provide a powerful complement to more conventional wind-retrieval techniques. This capability should be especially useful in littoral waters such as the continental U.S. coast including Alaska where accurate environmental monitoring is both extremely important and difficult to achieve. In this paper, we have provided an initial quantitative validation of high-resolution SAR wind retrieval through comparisons with model and buoy wind-speed measurements. Although there is much work yet to be done, we believe the results of these comparisons are quite promising and that further efforts to combine SAR image data with other meteorological data and model output could eventually lead to the availability of high-resolution wind estimates on an operational basis.

References

[1] R. W. Fett, "The Kamishak Gap wind as depicted in DMSP and SSM/I data," *Int. J. Remote Sensing*, vol. 14, no. 3, pp. 403–423, 1993.

[2] R. K. Raney, A. P. Luscombe, E. J. Langham, and S. Ahmed, "RADARSAT," *Proc. IEEE*, vol. 79, no. 6, pp. 839–849, June 1991.

[3] W. G. Pichel and P. Clemente-Colón, "NOAA coastwatch SAR applications and demonstration," *The Johns Hopkins Univ. Tech. Dig.*, vol. 21, pp. 49–57, Jan. 2000.

[4] R. C. Beal, "Toward an international stormwatch using wide-swath SAR," *The Johns Hopkins Univ. Tech. Dig.*, vol. 21, pp. 12–20, Jan. 2000.

[5] F. M. Monaldo, "The Alaska SAR demonstration and near real-time synthetic aperture radar winds," *The Johns Hopkins Univ. Tech. Dig.*, vol. 21, pp. 75–84, Jan. 2000.

[6] A. Stoffelen and D. L. T. Anderson, "ERS-1 scatterometer data characteristics and wind retrieval skill," *Adv. Space Res.*, vol. 13, pp. 553–560, 1993.

[7] D. R. Thompson, T. M. Elfouhaily, and B. Chapron, "Polarization ratio for microwave backscattering from the ocean surface at low to moderate incidence angles," in *Proc. IGARSS'99*, Lincoln, NE, July 1999, pp. 1671–1673.

[8] D. R. Thompson and R. C. Beal, "Mapping high-resolution wind fields using synthetic aperture radar," *The Johns Hopkins Univ. Tech. Dig.*, vol. 21, pp. 58–67, Jan. 2000.

[9] T. Elfouhaily, D. R. Thompson, D. Vandemark, and B. Chapron, "A new bistatic model for electromagnetic scattering from perfectly conducting random surfaces," *Waves in Random Media*, vol. 9, pp. 281–294, 1999.

[10] C. M. H. Unal, P. Snooji, and P. J. F. Swart, "The polarization-dependent relation between radar backscatter from the ocean surface and wind vectors at frequencies between 1 and 18 GHz," *IEEE Trans. Geosci. Remote Sens.*, vol. 29, pp. 621–626, May 1991.

[11] P. W. Vachon and F. W. Dobson, "Wind retrieval from RADARSAT SAR images: Selection of a suitable C-band HH polarization wind retrieval model," *Can. J. Remote Sensing*, vol. 26, pp. 306–313, Aug. 2000.

[12] J. Horstmann, W. Kock, S. Lehner, and R. Tonboe, "Wind retrieval over the ocean using synthetic aperture radar with C-band HH polarization," *IEEE Trans. Geosci. Remote Sens.*, vol. 38, pp. 2122–2131, Sept. 2000.

[13] J. Horstmann, S. Lehner, W. Kock, and R. Tonboe, "Computation of wind vectors over the ocean using spaceborne synthetic aperture radar," *The Johns Hopkins Univ. Tech. Dig.*, vol. 21, pp. 100–107, Jan. 2000.

[14] T. W. Gerling, "Structure of the surface wind field from the seasat SAR," *J. Geophys. Res.*, vol. 91, no. C2, pp. 2308–2320, 1996.

[15] F. Fetterer, D. Gineris, and C. C. Wackerman, "Validating a scatterometer wind algorithm for ERS-1 SAR," *IEEE Trans. Geosci. Remote Sens.*, vol. 36, pp. 479–492, Mar. 1998.

[16] G. Müller, B. Brümmer, and W. R. Alpers, "Roll convection with an artic cold-air outbreak: Interpreation of in situ aircraft measurements and spacecraft SAR imagery by a three-dimensional atmospheric model," *Mon. Weath. Rev.*, vol. 127, pp. 363–380, 1999.
[17] C. C. Wackerman, "Estimating wind vectors from RADARSAT synthetic aperture radar imagery," Tech. Rep. 10 032 100-1-T, Veridian ERIM Int., Ann Arbor, MI, 2000.
[18] P. D. Mourad, D. R. Thompson, and D. C. Vandemark, "Extracting fine-scale wind fields from synthetic aperture radar images of the ocean surface," *The Johns Hopkins Univ. Tech. Dig.*, vol. 21, pp. 108–115, Jan. 2000.
[19] P. W. Vachon, A. L. Gray, C. E. Livingston, and A. P. Luscombe, "Adaptive compensation of radarsat SAR analogue-to-digital converter saturation power loss," in *Geomatics in Era of RADARSAT, (GER 1997)*, Ottawa, ON, Canada, May 1997, pp. 27–30.
[20] P. W. Vachon, P. Adlakha, H. Edel, M. Henschel, B. Ramsay, D. Flett, M. Ray, G. Staples, and S. Thomas, "Canadian progress toward marine and coastal applications of synthetic aperture radar," *The Johns Hopkins Univ. Tech. Dig.*, vol. 21, pp. 33–40, Jan. 2000.
[21] F. M. Monaldo, "Expected difference between buoy and radar altimeter estimates of wind speed and significant wave height and their implicatons on buoy-altimeter comparisons," *J. Geophys. Res.*, vol. 93, no. C3, pp. 2285–2302, Mar. 1988.
[22] D. B. Gilhousen, "A field evaluation of NDBC moored buoy winds," *J. Atmos. Ocean. Technol.*, vol. 94, p. 104, 1987.
[23] C. W. Fairall, E. F. Bradley, D. P. Rogers, J. B. Edson, and G. S. Young, "Bulk parameterization of the air-sea fluxes for tropical ocean-global atmosphere response experiment," *J. Geophys. Res.*, vol. 101, no. C2, pp. 3747–3764, Feb. 1996.
[24] E. Attema, Y.-L. Desnos, and G. Duchossios, "Synthetic aperture radar in Euorpe: ERS, ENVISAT and beyond," *The Johns Hopkins Univ. Tech. Dig.*, vol. 21, pp. 155–161, Jan. 2000.
[25] R. Romeiser, W. Alpers, and V. Wissmann, "An improved composite model for the radar backscattering cross section of the ocean surface; 1. Theory and model validation/optimization by scatterometer data," *J. Geophys. Res.*, vol. 102, no. C5, pp. 25 237–25 250, May 1997.

Frank M. Monaldo received the B.A. and M.S. degrees from the Catholic University of America, Washington, DC, in 1977 and 1978, respectively.

He is currently a Principal Staff Physicist with the Johns Hopkins University Applied Physics Laboratory, Laurel, MD. He has focused on the scientific use of remotely sensed data from both passive and active sensors to measure geophysical properties of the ocean and atmosphere. This work has encompassed the theoretical development of remote sensing techniques and the implementation and validation of these techniques. He has published extensively on the use of radar altimetry, synthetic aperture radar (SAR) imagery, and optical image processing to measure geophysical properties. He was formerly the Program Scientist for the Geosat Follow-On Mission and a member of the Shuttle Imaging Radar Science Team.

Mr. Monaldo is a member of the American Geophysical Union, URSI Commission F, Sigma Xi, and the American Meteorological Society. He also serves on the AMS Committee for Satellite Meteorology and Oceanography and Alaska SAR Facility User Working Group. Most recently, he has developed a system for converting SAR imagery into real-time estimates of wind speed as part of the Alaska SAR Demonstration Project.

Donald R. Thompson received the B.S. degree in physics from Case Western Reserve University, Cleveland, OH, in 1964, and the Ph.D. degree in theoretical physics from the University of Minnesota, Minneapolis, in 1968.

He spent two years studying problems in stellar nucleosynthesis at the California Institute of Technology, Pasadena, before returning to the University of Minnesota in 1970. From 1976 to 1978, he was an Alexander von Humboldt Fellow with the Institut fuer Theoretiche Physik, Universitaet Tuebingen, Tuebingen, Germany. Since coming to The Johns Hopkins University Applied Physics Laboratory, Laurel, MD, in 1980, his research has been concerned with the physics of ocean surface waves and electromagnetic scattering from the ocean surface.

Robert C. Beal received the B.S. degree in electrical engineering from the Massachusetts Institute of Technology, Cambridge, and the M.S. degree in physics and astronomy from the University of Maryland, College Park, in 1961 and 1968, respectively.

In 1980, he was a Parsons Fellow in oceanography at The Johns Hopkins University, Baltimore, MD. He recently retired as The Johns Hopkins University Applied Physics Laboratory's (APL) Principal Professional Staff and Head of the Ocean Observations Section of the Space Department's Ocean Remote Sensing Group. He has been interested in the problem of measuring winds and waves from space since 1974, in the early study phase of Seasat. He has been a Principal Investigator for several SAR oceanography and research programs sponsored by NOAA, NASA, and the Navy, including Seasat, SIR-B, SIR-C, ERS-1, and Radarsat. He led a successful APL effort to implement a real-time SAR spectral processor which flew on the SIR-C mission. His present interests continue to be the application of spaceborne SAR to oceanography and meteorology.

William G. Pichel received the B.S. degree in physics from the University of Florida, Gainesville, in 1969, and the M.S. degree in physical oceanography from the University of Hawaii, Honolulu, in 1979.

He has been with the National Environmental Satellite, Data and Information Service of the National Oceanic and Atmospheric Administration, Washington, DC, since 1970. His assignments have included Product Area Leader for Oceanographic Products, Chief of the Product Systems Branch and currently, Research Physical Scientist with the Oceanic Research and Applications Division of the Office of Research and Applications. His research interests include development of ocean and hydrologic applications of synthetic aperture radar data and the improvement of sea surface temperatures from satellite infrared measurements.

Dr. Pichel has received three Department of Commerce Bronze Medals for his contributions to the development and demonstration of new satellite ocean remote sensing applications.

Pablo Clemente-Colón received the B.S. degree in physics at the University of Puerto Rico, Mayaguez, in 1977, the M.S. degree in oceanography from Texas A&M University, College Station, in 1980, and the Ph.D. degree in oceanography from the University of Delaware, Newark, in 2001.

He is currently an Oceanographer with the National Oceanic and Atmospheric Administration (NOAA) National Environmental Satellite, Data and Information Service (NESDIS) Office of Research and Applications, Washington, DC, and is also a Research Associate in ocean remote sensing with the University of Delaware, Newark. His research interests include satellite oceanography, operational sea surface temperature monitoring, synthetic aperture radar (SAR), coastal applications, upper ocean dynamics, ocean color, remote sensing fisheries, marine boundary processes, and data fusion.